OMTN, Volume *21*

Supplemental Information

METTL3 Induces AAA Development and Progression by Modulating N6-Methyladenosine-Dependent Primary miR34a Processing

Lintao Zhong, Xiang He, Haoyu Song, Yili Sun, Guojun Chen, Xiaoyun Si, Jie Sun, Xiaoqiang Chen, Wangjun Liao, Yulin Liao, and Jianping Bin

METTL3 induces abdominal aortic aneurysm development and progression by modulating N6-methyladenosine-dependent primary miR34a processing

Lintao Zhong [a,*], MD, PhD; Xiang He[a], MD, PhD; Haoyu Song[a], MD, PhD; Yili Sun [a], MD, PhD; Guojun Chen[a], MD, PhD; Xiaoyun Si [a], MD, PhD; Jie Sun[a], MD, PhD; Xiaoqiang Chen[a], MD; Wangjun Liao[b], MD, PhD; Yulin Liao[a], MD, PhD; Jianping Bin[a, *], MD, PhD

[a] State Key Laboratory of Department of Cardiology, Organ Failure Research, Nanfang Hospital, Southern Medical University, Guangzhou 510515, China;
[b] Department of Oncology, Nanfang Hospital, Southern Medical University, Guangzhou 510515, China

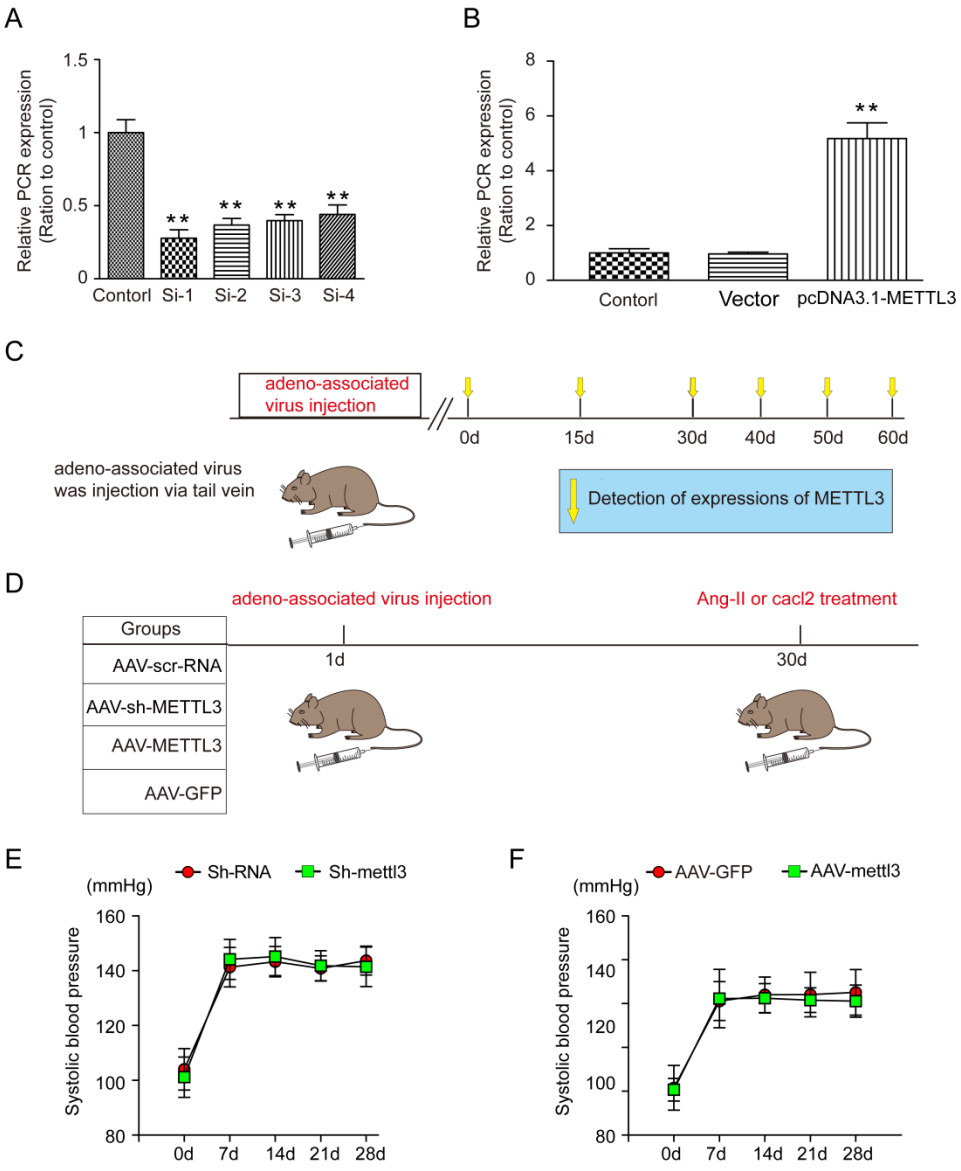

Online Figure 1

Online Figure 1. Selection of a potent adeno-associated virus (AAV) carrying METTL3 siRNA and overexpression plasmids and a diagram of the virus-related experimental flow. A, Inhibitory effects of four small interfering RNAs (siRNAs) against METTL3 in VSMCs as assessed by qRT-PCR analysis. B, Overexpression effects of the constructed pcDNA3.1-METTL3 plasmid in VSMCs as assessed by qRT-PCR analysis. C, Protocol for the in vivo AAV-mediated METTL3 knockdown and overexpression experiment. A predetermined number of male mice were injected with Scr-RNA, sh-METTL3, AAV-GFP or AAV-METTL3. Before injection and at 15 days, 30 days, 40 days, 50 days, and 60 days after the initial injection, a predetermined number of mice were sacrificed, and aortic samples were collected to detect aortic METTL3 expression (n=3). D, Thirty days after the initial AAV transfection, mice were treated with Ang II via minipump for four weeks or were

subjected to $CaCl_2$-treatment surgery and sacrificed after 3 or six weeks. The data are presented as the mean ± SD. *P<0.05, **P<0.01.

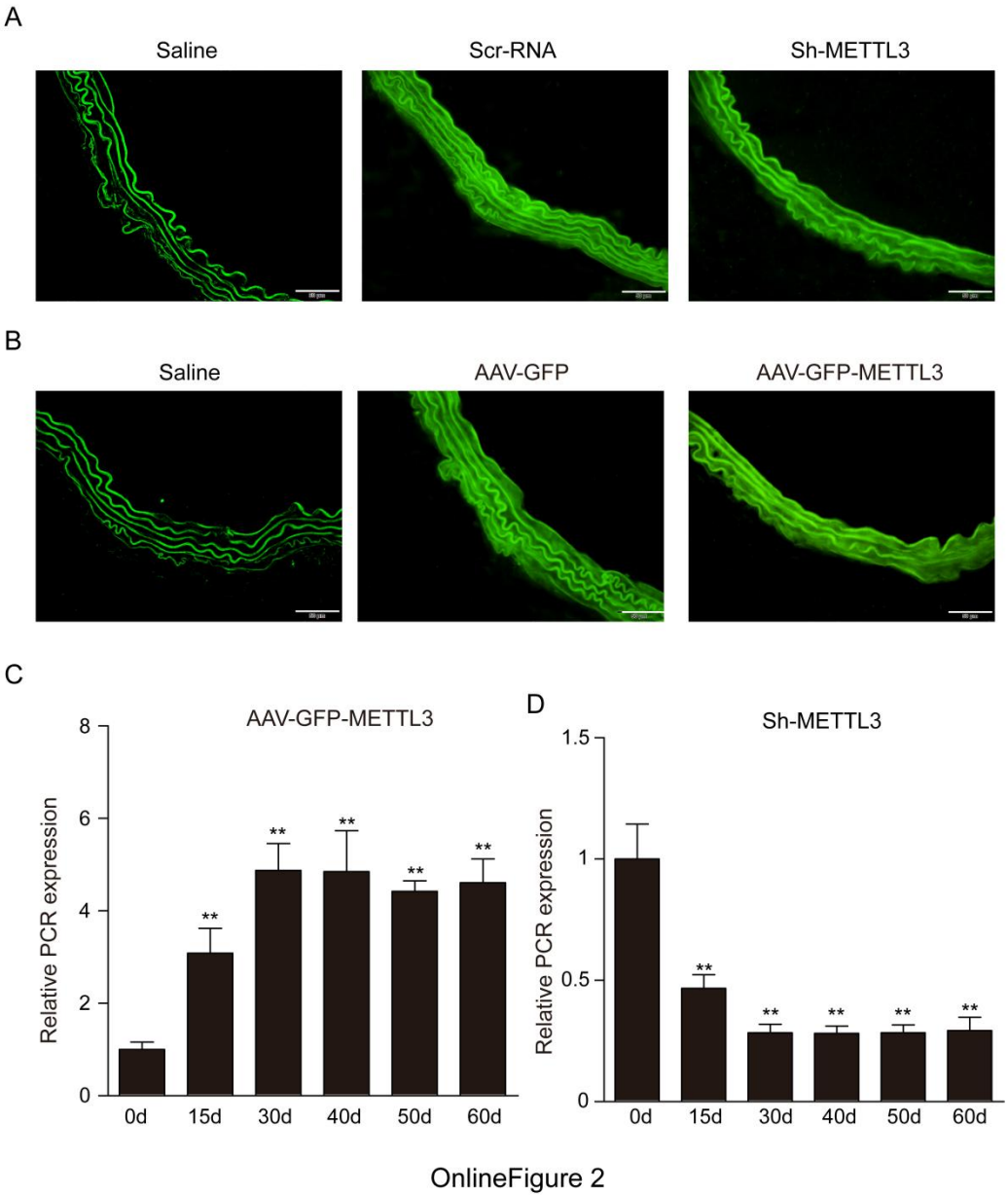

Online Figure 2. Confirmation of the viral infection efficiency in the suprarenal aortas of mice. A and B, Representative immunofluorescent staining of virus-borne green fluorescent protein (GFP) in the aortas of mice from the different virus-mediated groups and the saline group (scale bar, 50 μm). C and D, qRT-PCR analysis of the mRNA expression of METTL3 over time after sh-METTL3 or AAV-METTL3 transfection in the suprarenal aortas of mice (n=3). The data are presented as the mean ± SD. *P<0.05.

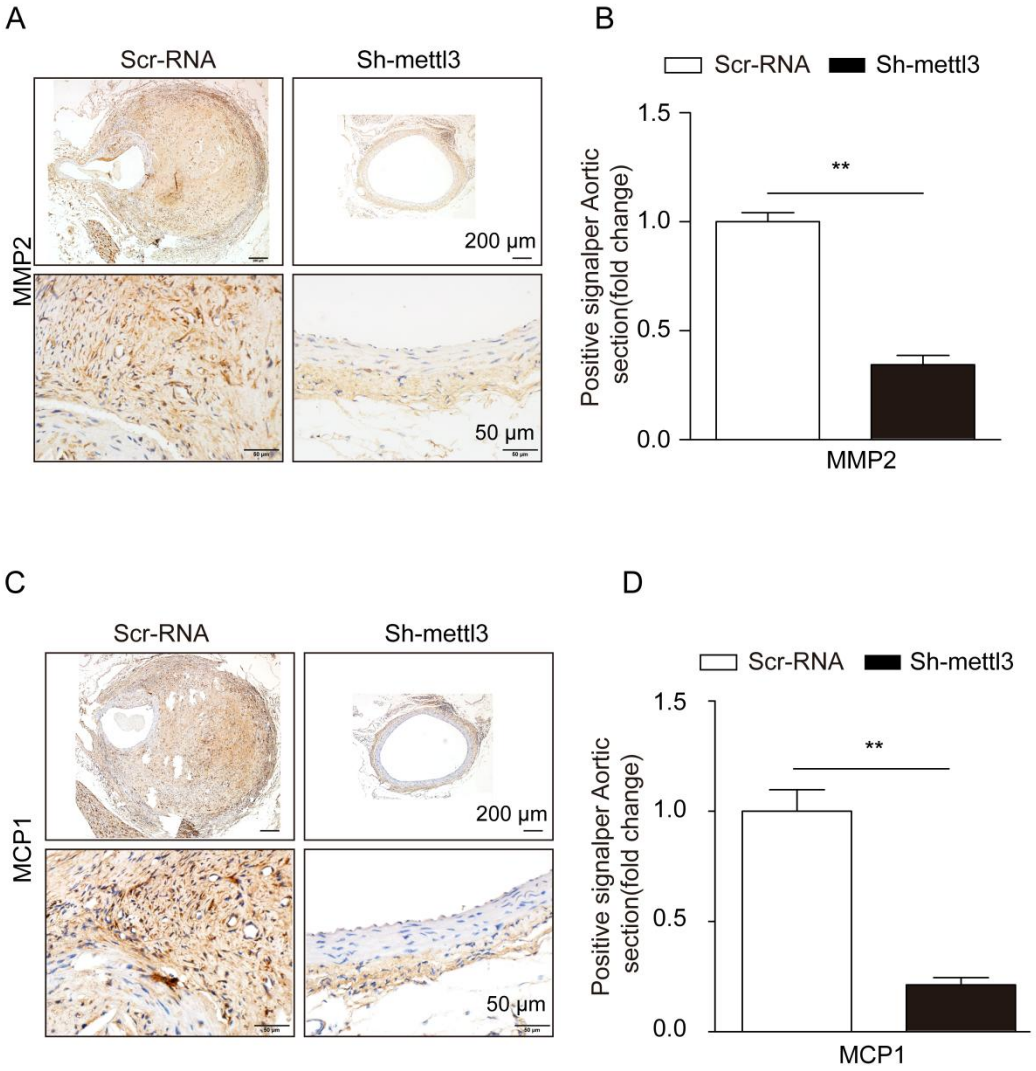

Online Figure 3

Online Figure 3. METTL3 knockdown attenuates MMP2 and MCP1 expression in Ang II-infused ApoE$^{-/-}$ mice. A to D, Immunohistochemical staining of abdominal aortic MMP2 (A,B) and MCP1 (C,D) in Ang II-infused male ApoE-/- mice (n=3; scale bars, 200 μm (upper) and 50 μm (lower)). The data are presented as the mean ± SD. *P<0.05.

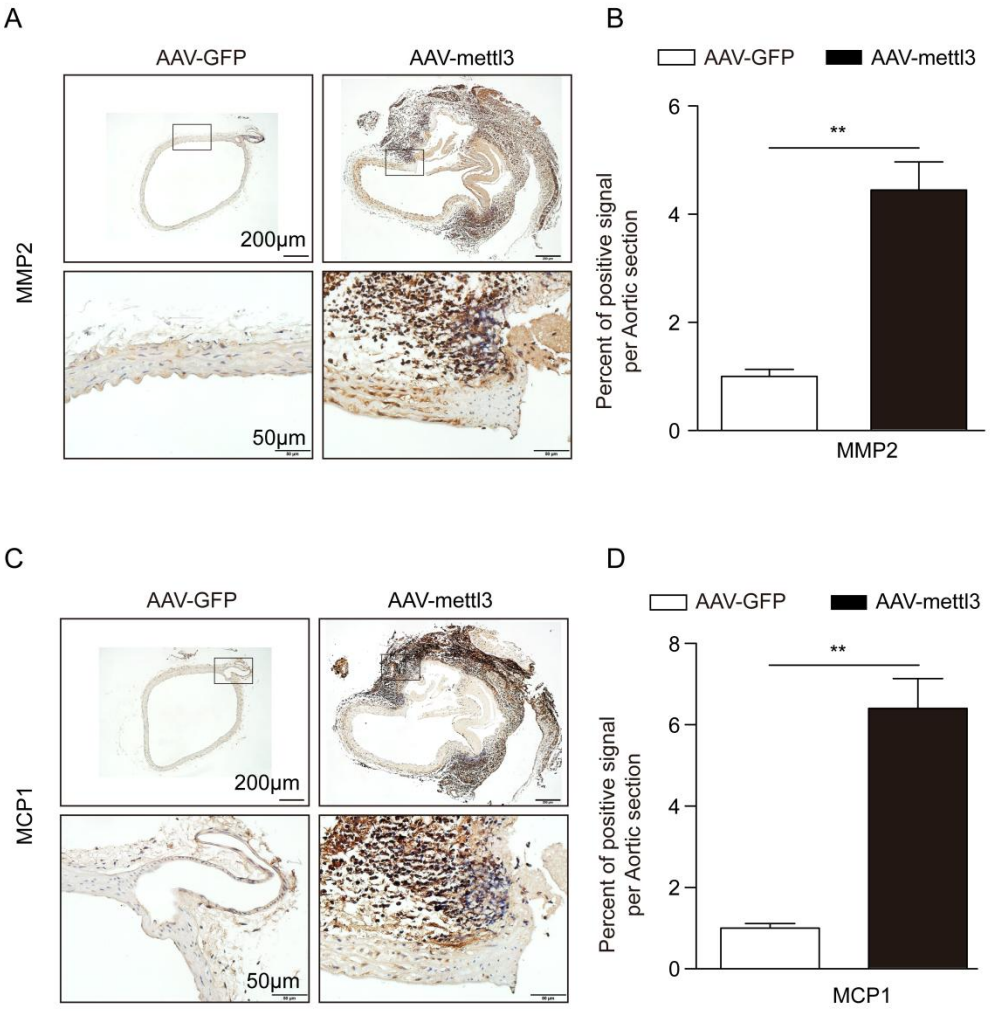

Online Figure 4

Online Figure 4. Overexpression of METTL3 increases the expression of MMP2 and MCP1 in Ang II-infused C57BL/6J mice. A to D, Immunohistochemical staining of abdominal aortic MMP2 (A,B) and MCP1 (C,D) in Ang II-infused C57BL/6J mice (n=3; scale bars, 200 μm (upper) and 50 μm (lower)). The data are presented as the mean ± SD. *P<0.05.

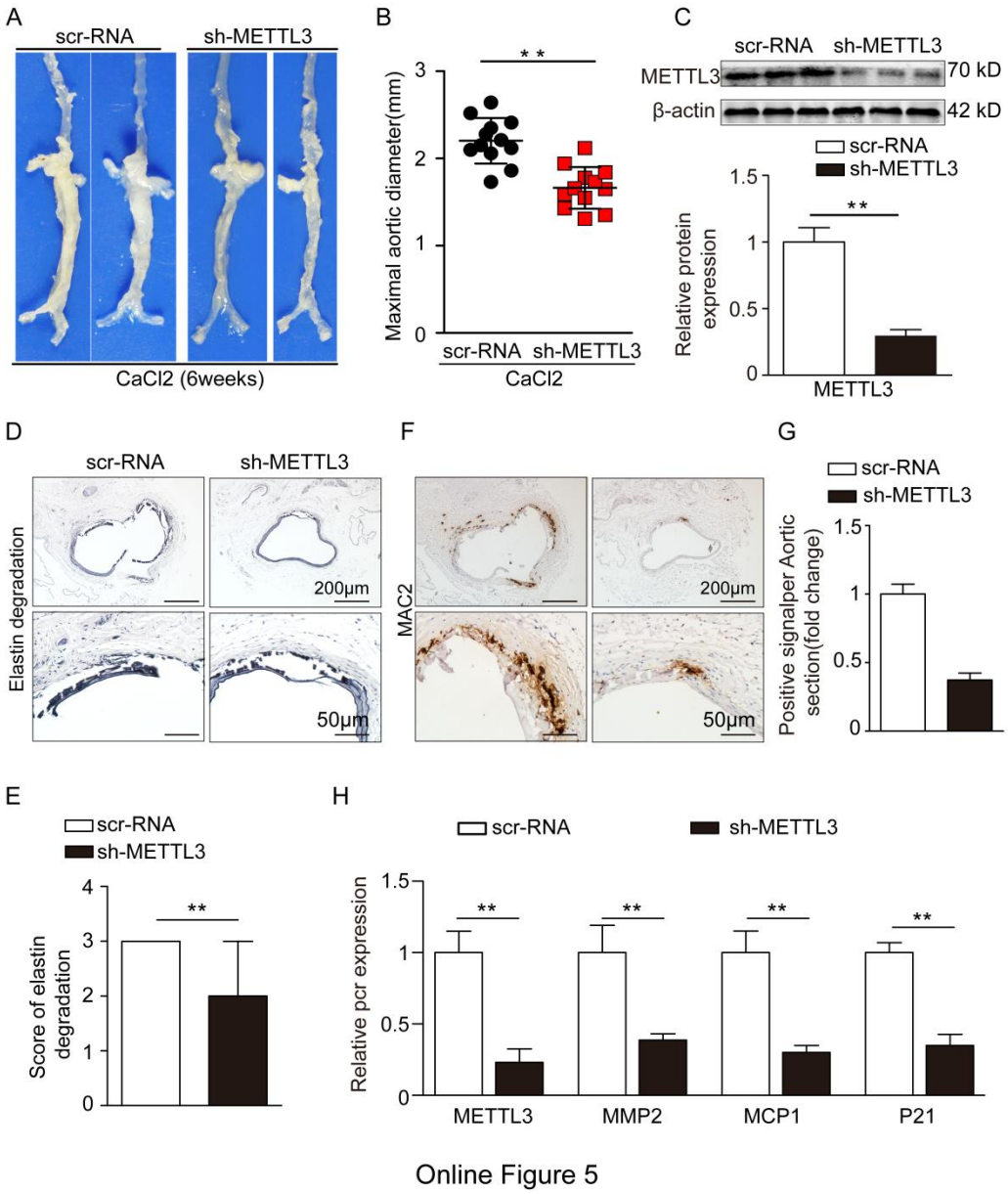

Online Figure 5

Online Figure 5. METTL3 suppression inhibits CaCl2-induced AAA formation. C57BL/6J mice were injected with Scr-RNA or sh-METTL3, and their infrarenal aortas were then treated with $CaCl_2$ for 15 min. After six weeks, the mice were sacrificed and used for analysis. A, Representative images showing C57BL/6J mouse infrarenal aortas treated with $CaCl_2$. B, Maximal diameters of infrarenal aortas from $CaCl_2$-induced C57BL/6J mice. C, Representative western blots and statistical analysis of aortic METTL3 in $CaCl_2$-treated C57BL/6J mice. D and E, Representative elastin staining and statistical analysis of elastin degradation scores in the two groups of mice. F and G, Representative immunohistochemical staining (F) and statistical analysis (G) of MAC2 in aortas from the two groups of mice (n=4 per group). G and H, mRNA levels of aortic METTL3, MCP-1, MMP-2 and P21 in $CaCl_2$-treated C57BL/6J mice. The data are presented as the mean ± SD. *P<0.05, **P<0.01.

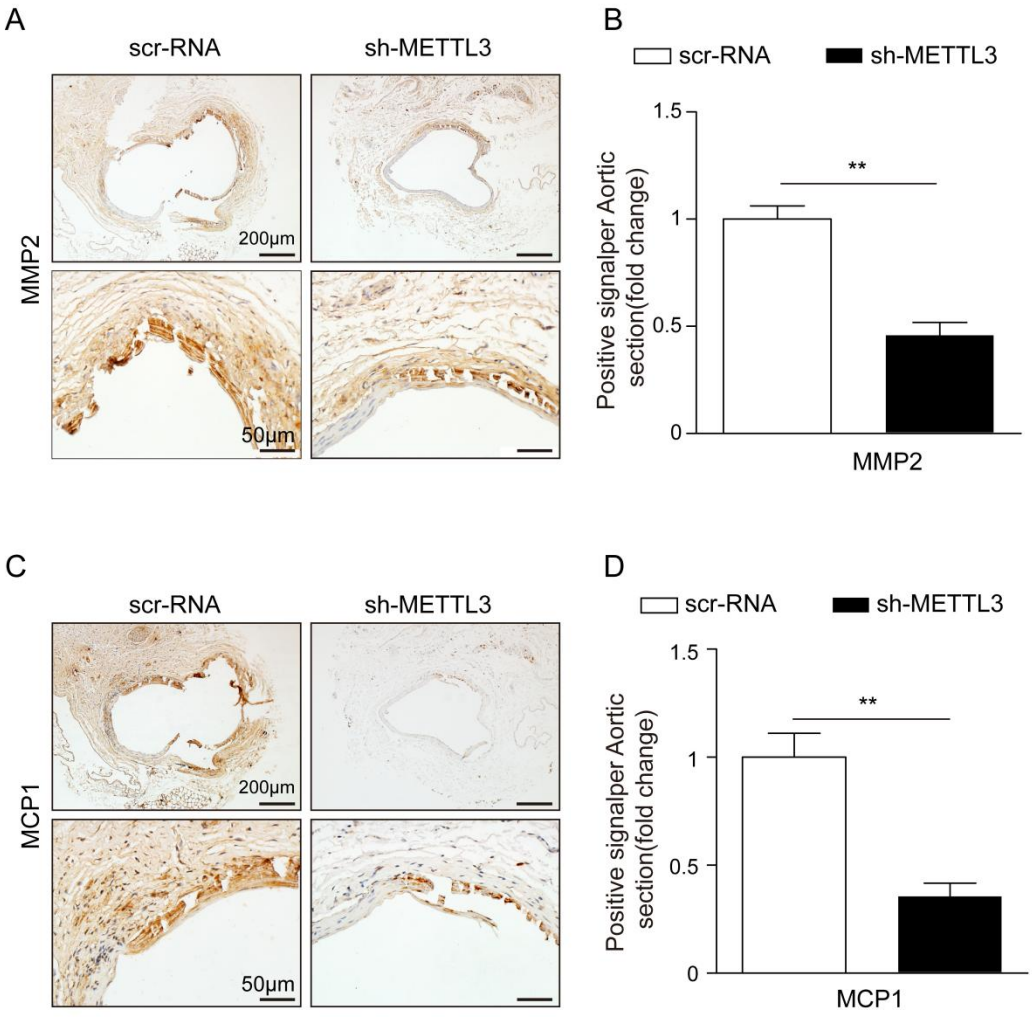

Online Figure 6

Online Figure 6. METTL3 suppression inhibits vascular MMP2 and MCP1 expression. A to C**,** Immunofluorescent staining for MMP2 (A,B) and MCP1 (C,D) (scale bars, 200 μm (upper) and 50 μm (lower)). The data are presented as the mean ± SD. **P*<0.05.

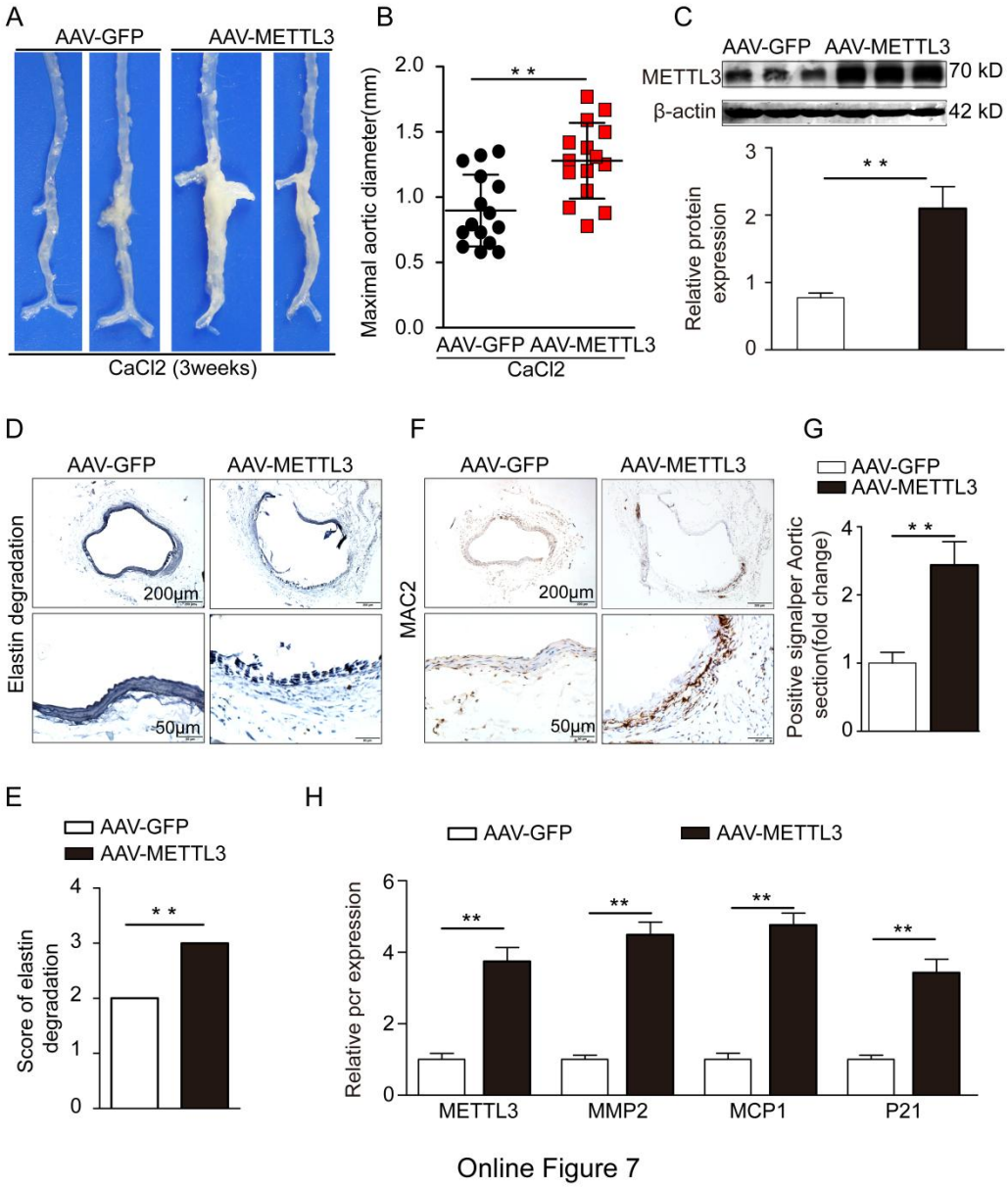

Online Figure 7

Online Figure 7. METTL3 overexpression exacerbates $CaCl_2$-induced AAA formation. C57BL/6J mice were injected with AAV-GFP or AAV- METTL3, and their infrarenal aortas were then treated with $CaCl_2$ for 15 min. After three weeks, the mice were sacrificed and used for analysis. A, Representative images showing C57BL/6J mouse infrarenal aortas treated with $CaCl_2$. B, Maximal diameters of infrarenal aortas from $CaCl_2$-induced C57BL/6J mice. C, Representative western blots and statistical analysis of aortic METTL3 in $CaCl_2$-treated C57BL/6J mice. D and E, Representative elastin staining and statistical analysis of elastin degradation scores in the two groups of mice. F and G, Representative immunohistochemical staining (F) and statistical analysis (G) of MAC2 in aortas from the two groups of mice (n=4 per group). G and H, mRNA levels of aortic METTL3, MCP-1, MMP-2 and P21 in $CaCl_2$-treated C57BL/6J mice. The data are presented as the mean ± SD. *P<0.05, **P<0.01.

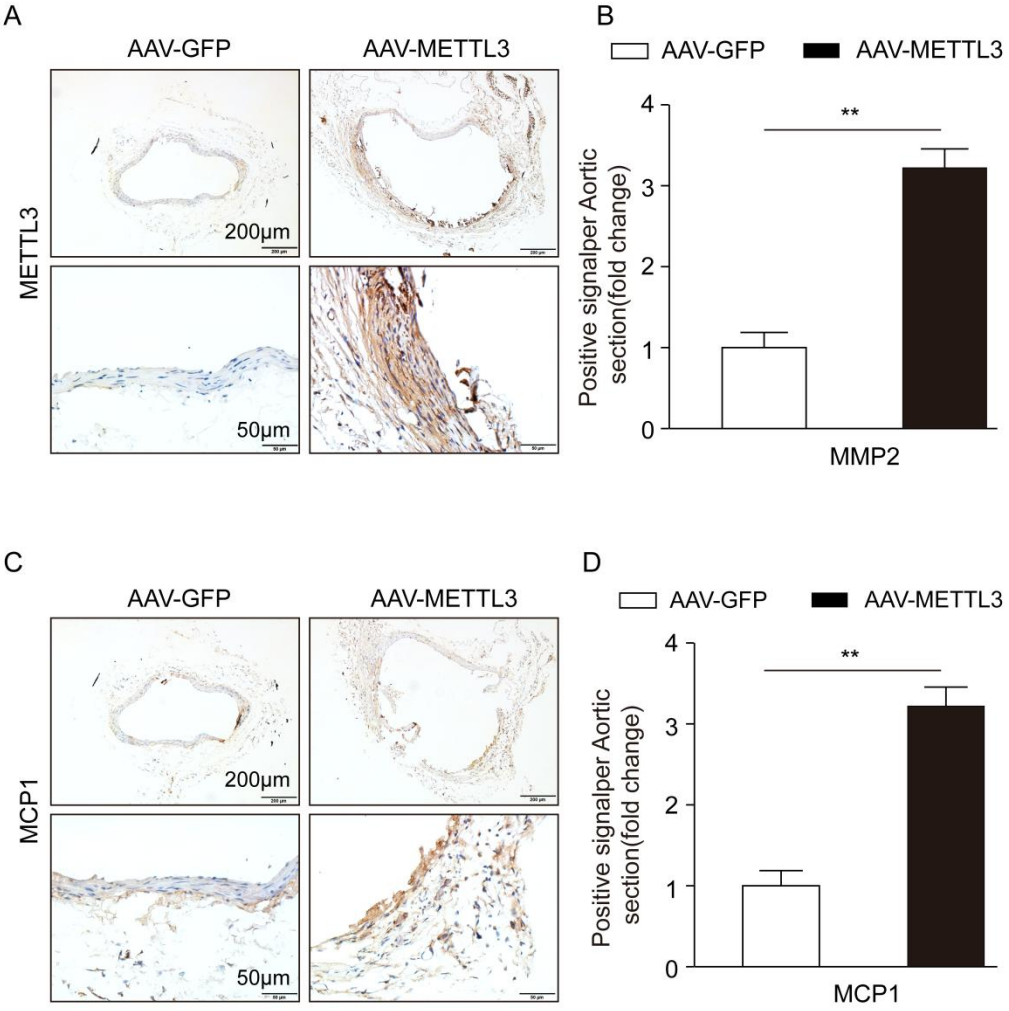

Online Figure 8

Online Figure 8. METTL3 overexpression increases vascular MMP2 and MCP1 expression. A to D**,** Immunofluorescent staining for MMP2 (A,B) and MCP1 (C,D) (scale bars, 200 μm (upper) and 50 μm (lower)). The data are presented as the mean ± SD. **P*<0.05, **P<0.01.

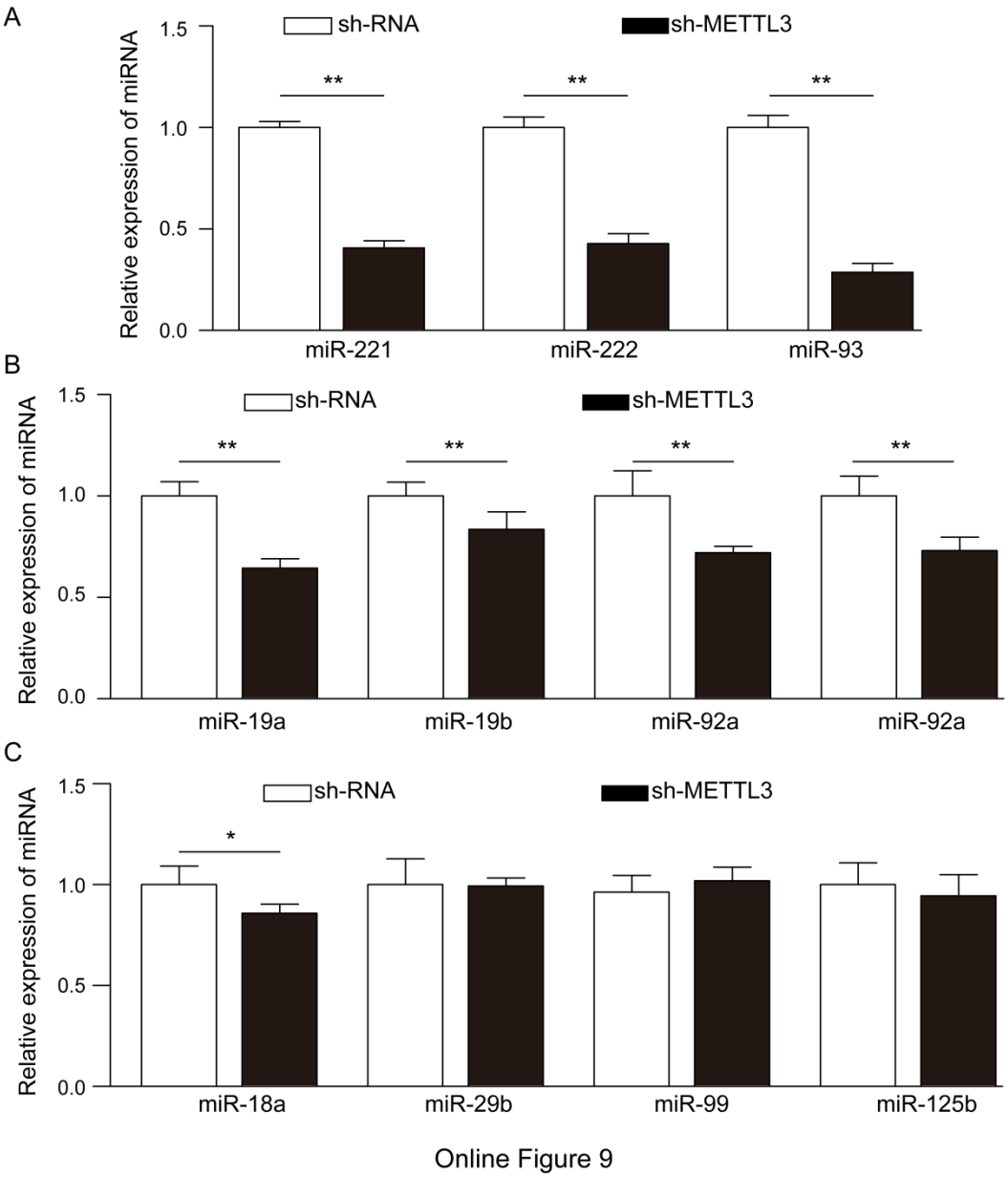

Online Figure 9. Expression of miRNAs in METTL3-depleted SMCs. A, miR-34a, miR-221, miR-222 and miR-93 were quantified by qRT-PCR upon METTL3 depletion in SMCs. B, miR-19a, miR-19b, miR-92a and miR-20a were quantified by qRT-PCR upon METTL3 depletion in SMCs. C, miR-18a, miR-29b, miR-99 and miR-125b were quantified by qRT-PCR upon METTL3 depletion in SMCs. Abbreviations: siRNA, small interfering fragment control; sh-METTL3, METTL3 knockdown. The data are presented as the mean ± SD. *P<0.05, **P<0.01.

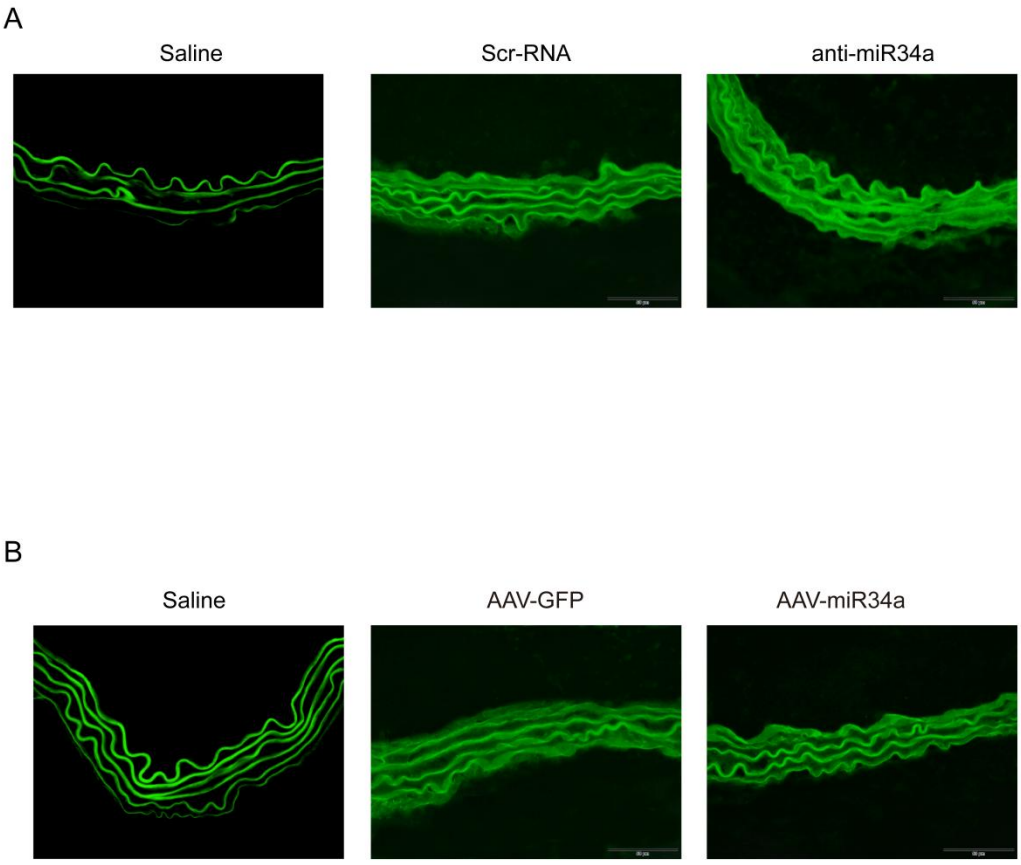

Online Figure 10

Online Figure 10. Confirmation of the transfection efficiency of anti-miR34a, AAV-miR34a, and control sequences in the suprarenal aortas of mice. A and B, Representative immunofluorescent staining of virus-borne green fluorescent protein (GFP) in the aortas of mice from the different virus-mediated groups and the saline group (scale bar, 50 μm).

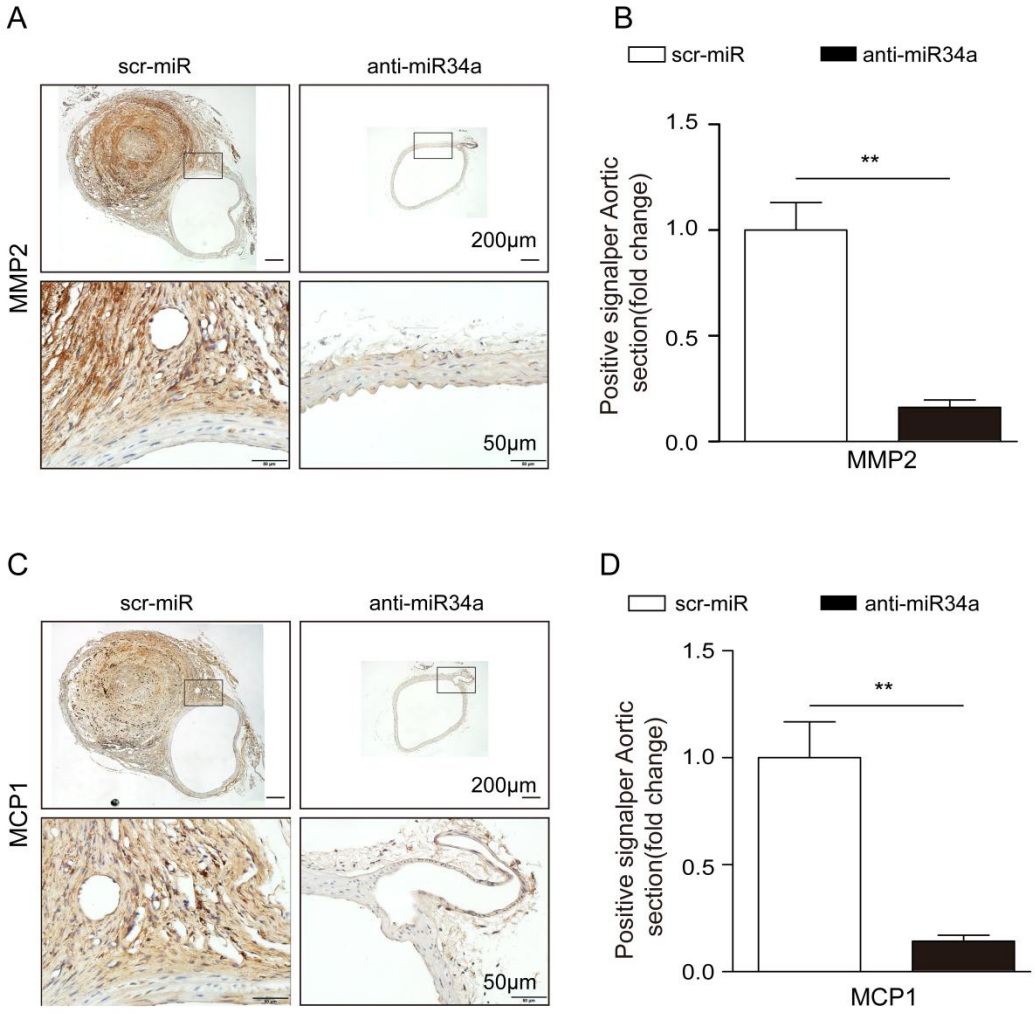

Online Figure 11

Online Figure 11. miR34a knockdown inhibits vascular MMP2 and MCP1 expression. A to C**,** Immunofluorescent staining for MMP2 (A,B) and MCP1 (C,D) (scale bars, 200 μm (upper) and 50 μm (lower)). The data are presented as the mean ± SD. **P*<0.05, **P<0.01.

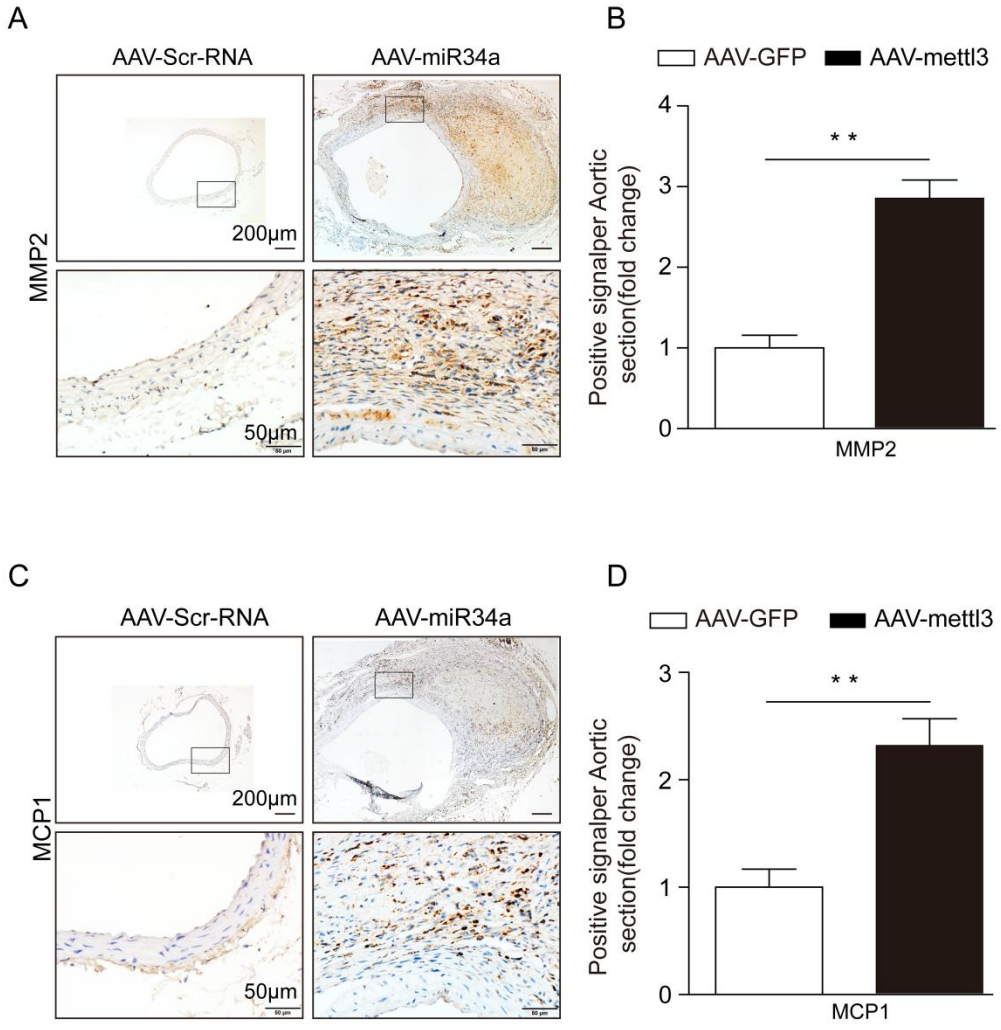

Online Figure 12

Online Figure 12. miR34a overexpression increases vascular MMP2 and MCP1 expression. A to D**,** Immunofluorescent staining for MMP2 (A,B) and MCP1 (C,D) (scale bars, 200 μm (upper) and 50 μm (lower)). The data are presented as the mean ± SD. **P*<0.05, **P<0.01.

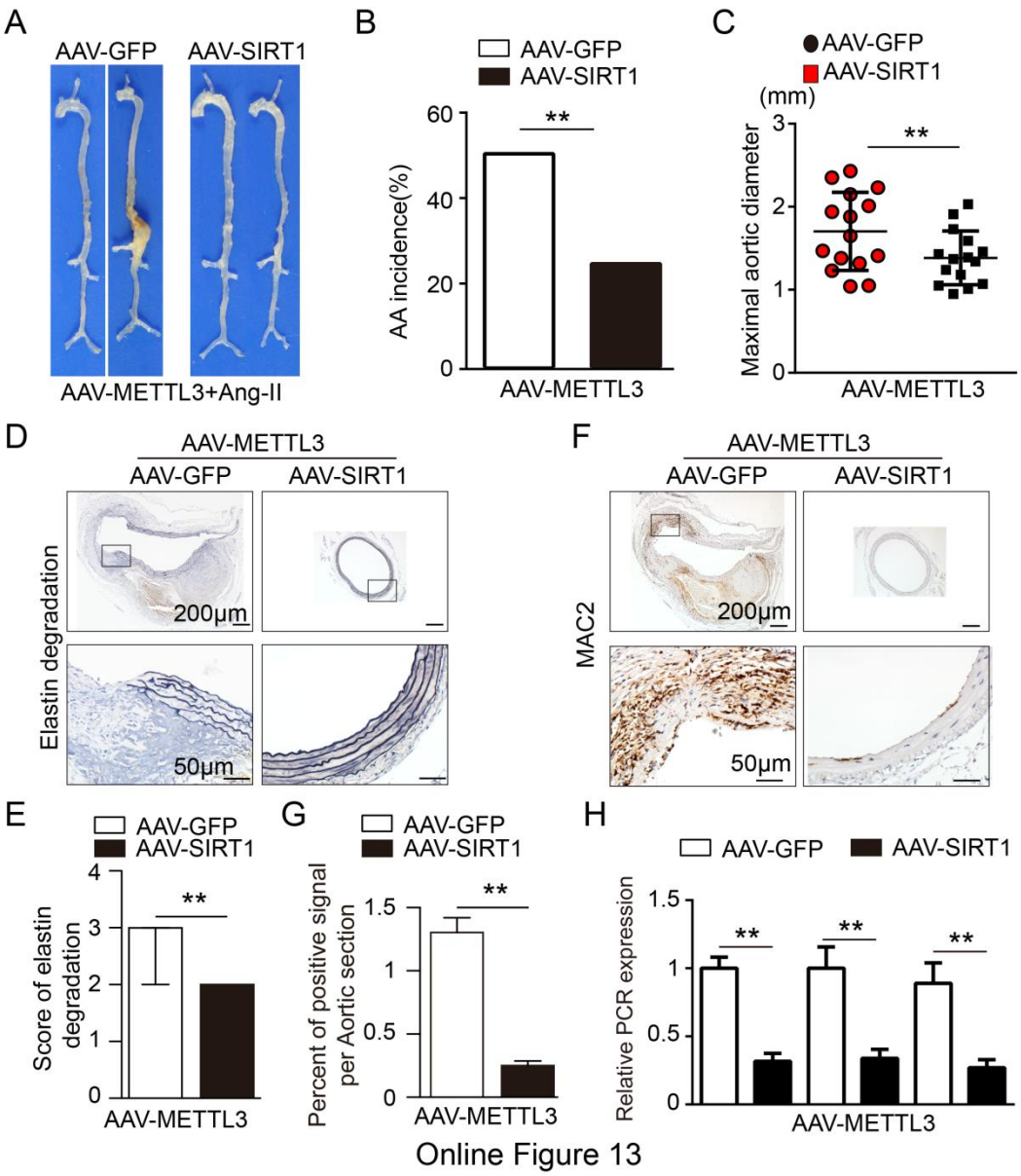

Online Figure 13. METTL3 overexpression promotes AAA via miR34a/SIRT1. A, Representative photographs of the macroscopic features of AAAs in AAV-METTL3 transfected Ang II-infused C57BL/6J mice in the AAV-GFP group or the AAV-SIRT1 group. B, Statistical analysis of AAA incidence in AAV-METTL3 transfected Ang II-infused C57BL/6J mice. C, Maximal aortic diameters in the AAV-METTL3-transfected Ang II-infused C57BL/6J mice in the two groups. D and E, Representative elastin staining and elastin degradation scores in suprarenal aortas from AAV-METTL3 transfected Ang II-infused C57BL/6J mice. The data are presented as the medians and quartiles. **P<0.01. F and G, Representative immunostaining for MAC2 (scale bars, 200 and 50 μm) and the corresponding densitometric analysis (n=3). H, Relative mRNA expression of MMP2, MCP1 and P21 in AAV-METTL3 transfected Ang II-infused C57BL/6J mouse aortas (n=4). The data are presented as the mean ± SD. *P<0.05, **P<0.01.

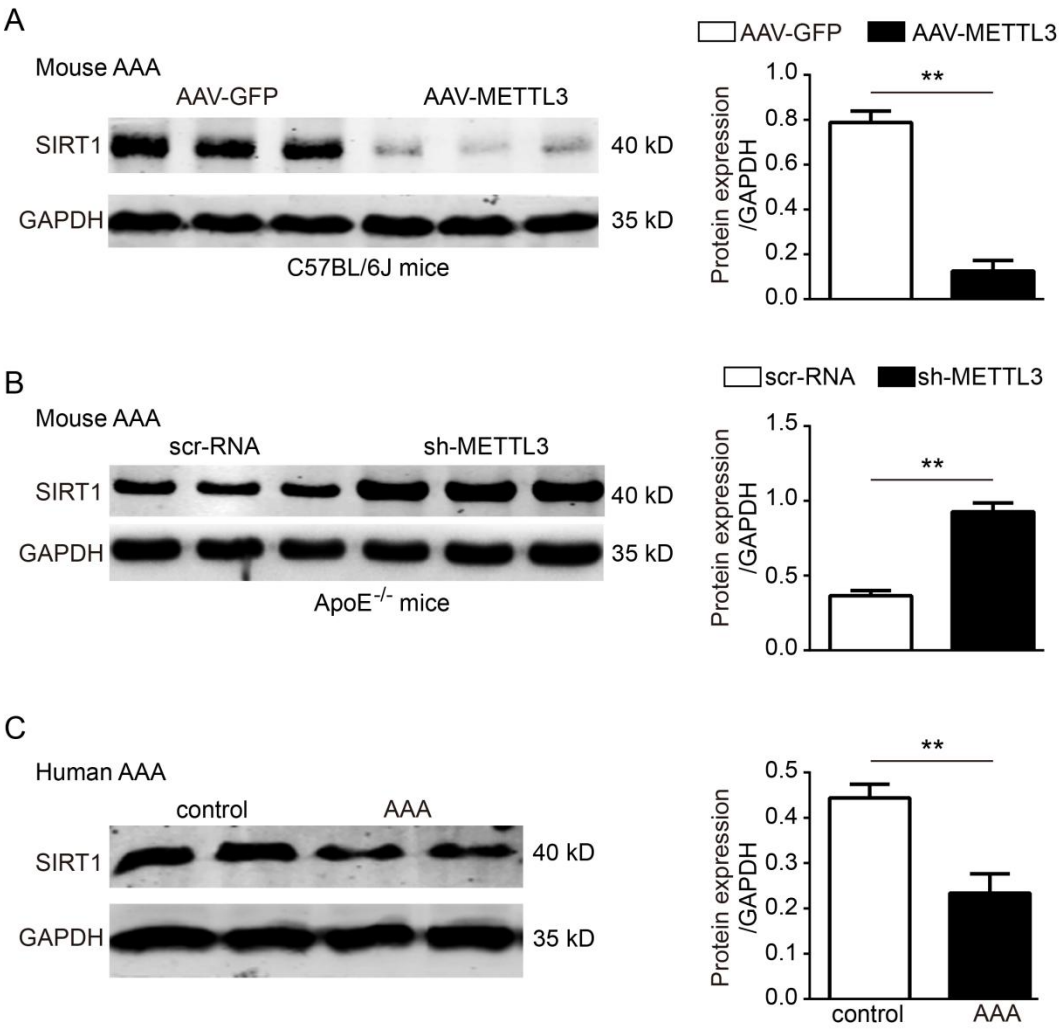

Online Figure 14. SIRT1 was substantially upregulated in METTL3 knockdown samples but downregulated in METTL3 overexpression samples. A, Western blot analysis of SIRT1 in Ang II-infused C57BL/6J mice in the AAV-GFP group or the AAV-METTL3 group (n=4). B, Western blot analysis of SIRT1 in Ang II-infused male $ApoE^{-/-}$ mice in the scr-RNA group or the sh-METTL3 group (n=4). C, Western blot analysis of SIRT1 in human AAA and adjacent nonaneurysmal aortic samples. **P<0.01.

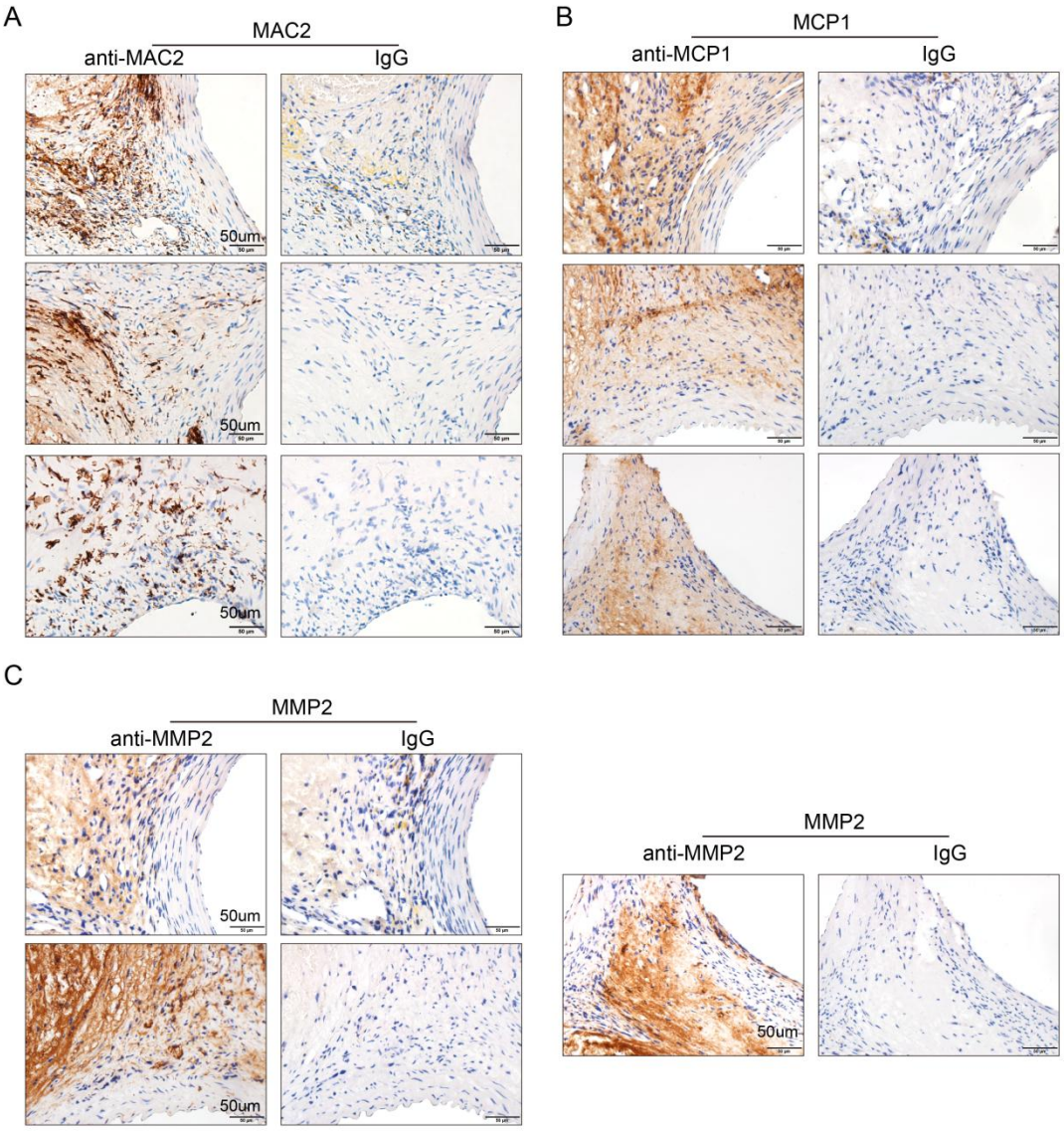

Online Figure 15

Online Figure 15. Negative control experiments confirming the specificity of antibody binding in the immunohistochemistry results. A to C, Representative images of immunohistochemical staining for MAC2 (A), MCP1 (B), and MMP2 (C) (scale bars, 50 μm).

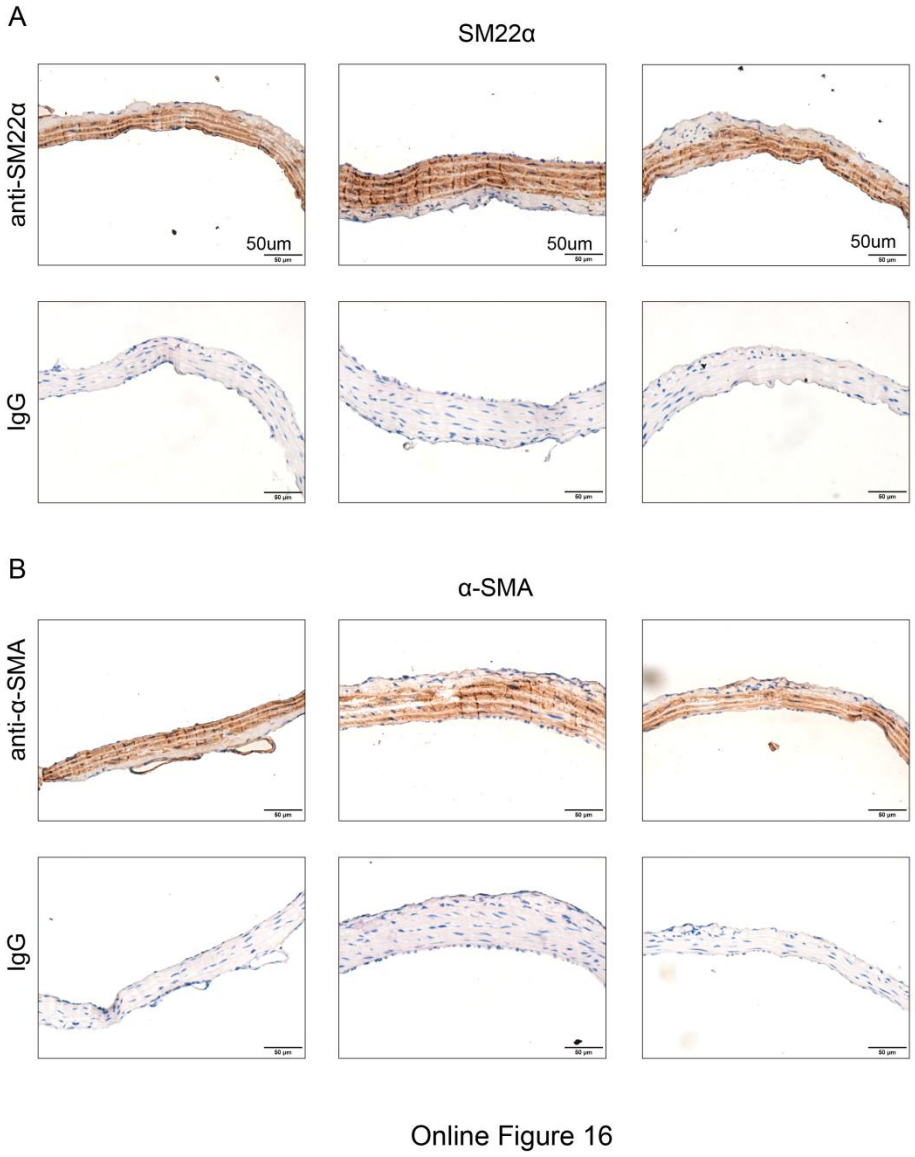

Online Figure 16

Online Figure 16. Negative control experiments confirming the specificity of antibody binding in the immunohistochemistry results. A and B, Representative images of immunohistochemical staining for SM22α (A) and α-SMA (B) (scale bars, 50 μm).

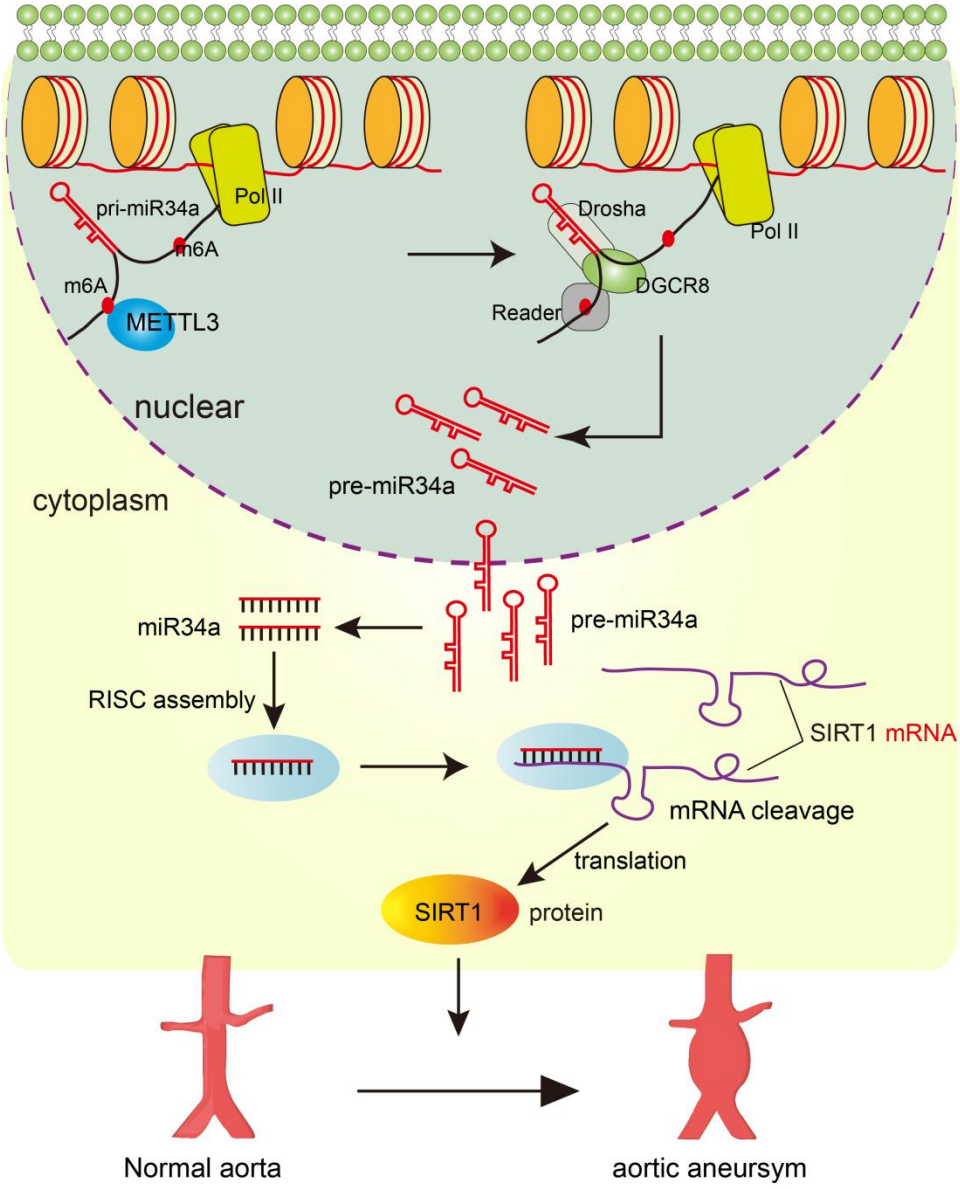

Online Figure 17

Online Figure 17. Working model of the role of METTL3 in AAA formation. METTL3 increases m^6A modification of pri-miR34a, which favors the binding of pri-miR34a to DGCR8. METTL3 promotes mature miR34a expression in a DGCR8-dependent manner, which leads to AAA formation through inhibition of SIRT1 expression.

Major Resources Tables

Table 1

Patient clinical information（n=5）

characteristics	AAA
Ever-smoker	100%
hypertensive	100%
hyperlipidemia	100%
coronary artery disease	80%
gender	male
average age	64.2±4.44 years

Table 2

Specific siRNAs against METTL3, miR34a and their nonspecific controls (NCs)

siMETTL3,sense:GCAUUGGUGCUGUGUUAAATTUUUAACACAGCACCAAU GCTT
siNC,sense: UUCUCCGAACGUGUCACGUTTACGUGACACGU UCGGAGAATT
Anti-miR-34a,sense: ACAACCAGCTAAGACACTGCCA
Scr-miR, sense: TTCTCCGAACGTGTCACGT

Table 3

Antibodies for immunohistochemistry analysis

name	Vendor or Source	Catalog #
anti-SM22α	Abcam	Ab170902
anti-αSMA	Abcam	ab32575
anti-MMP2	Abcam	ab37150
anti-MCP1	Thermo Fisher	PA5-34505
anti-MAC2	Abcam	ab76245
anti-IgG	Abcam	ab172730

Table 4

Antibodies for immunofluorescent analysis

name	Vendor or Source	Catalog #
anti- METTL3	Abcam	ab195352
anti- SM22α	Abcam	ab10135
Alexa Fluor 488	Abcam	ab150129
Alexa Fluor 594	Abcam	ab150088

Table 5

Antibodies for western blots

name	Vendor or Source	Catalog #
anti- METTL3	Abcam	ab195352
anti- MCP1	Thermo Fisher	PA5-34505
anti- MMP2	Abcam	ab37150
anti- P21	Abcam	Ab109119
anti- SM22α	Abcam	ab155272
anti- SIRT1	Abcam	ab110304
anti-β-actin	Abcam	ab5694
anti-GAPDH	Abcam	Ab9485

Table 6

Quantitative real-time PCR

Primer	Sequence (5'-3')
miR34AHG _forward	TGGCAGTGTCTTAGCTGGTTGT
miR34AHG _ reverse	TGGCGTCTCCCACTGGTCT
miR34a _forward	TGGCAGTGTCTTAGCTGGTTGT
miR34a _ reverse	AGTGCAGGGTCCGAGGTATT
U6 _forward	CTCGCTTCGGCAGCACA
U6 _ reverse	AACGCTTCACGAATTTGCGT
METTL3 _forward	TTCATCTTGGCTCTATCCGGC
METTL3_ reverse	GCACGGGACTATCACTACGG
METTL14 _forward	CCATAATGATTACTGCCAAC
METTL14 _ reverse	GTCAAAGGCTTCTATGTCTG
WTAP _forward	GCAACCAAAGAGCAGGAGAT
WTAP _ reverse	CTTCCAGGCACTCAGTTCAT
YTHDF2 _forward	TAGCCAGCTACAAGCACACC
YTHDF2_ reverse	TTTCCCACGACCTTGACGTT
FTO _forward	GAGCAGCCTACAACGTGACT
FTO _ reverse	GAAGCTGGACTCGTCCTCAC
KIAA1429 _forward	GCTGATGACTGCAATCTGCG
KIAA1429 _ reverse	CTCCACAACAGCCCATAGCA
METTL4 _forward	TTCGAAGTTAATCCAAGAAGG T
METTL4 _ reverse	CGTTTGAAGCTCCATTTCAT
ALKBH5 _forward	TGTGCTCAGTGGGTATGCTG
ALKBH5_ reverse	CTGACAGGCGATCTGAAGCA
MMP2 _forward	ACCAACACTGGGACCTGTCAC
MMP2_ reverse	CGAAGAACACAGCCTTCTCCT
MMP9 _forward	GCGTGTCTGGAGATTCGACTTG
MMP9_ reverse	ACTGCAGGAGGTCGTAGGTCAC
MCP1_forward	ACCTGCTGCTACTCATTCAC
MCP1_ reverse	CATTCAAAGGTGCTGAAGAC
β-actin _forward	GGCTGTATTCCCCTCCATCG
β-actin _ reverse	CCAGTTGGTAACAATGCCATGT

Table 7

(DGCR8) RIP-specific primer pairs for the miR34AHG gene

5’- TGGCAGTGTCTTAGCTGGTTGT -3’ (forward)
5’- TGGCGTCTCCCACTGGTCT -3’ (reverse)

Table 8

(m^6A) RIP-specific primer pairs for the miR34AHG gene

Site 1: 5’- ATGCCAACTTTGAGGCCA-3’ (forward)
Site 1: 5’- CTCTCCATCCTCCGGTGA-3’ (reverse)
Site 2 : 5’- ATGCCAACTTTGAGGCCA-3’ (forward)
Site 2 : 5’- AAGACCTGGGGAAGCCAC-3’ (reverse)
Site 3 : 5’-AAGAGGTGACGCCAAACG-3’ (forward)
Site 3 : 5’-CCTGGCCTGTGTGAAAGG-3’ (reverse)